Fundamental magnetization processes in nanoscaled composite permanent magnets

R. Fischer, T. Leineweber, and H. Kronmüller
Max-Planck-Institut für Metallforschung, Institut für Physik, Postfach 80 06 65, 70569 Stuttgart, Germany
(Received 17 April 1997; revised manuscript received 5 January 1998)

Excellent candidates for high remanent permanent magnets are nanoscaled composite materials consisting of soft magnetic α-Fe grains embedded into a hard magnetic $Nd_2Fe_{14}B$ environment. The magnetic properties of such permanent magnets sensitively depend on the prepared grain structure. This can be understood by computational micromagnetism, which reveals the relation between details of the grain structure and intergranular interaction mechanisms like the short-range exchange and the long-range stray field. The main problem of composite materials is to preserve a sufficiently high coercivity. This can be only guaranteed if the soft magnetic inclusions are smaller than twice the domain-wall width $\delta_B^{hard}=\pi\sqrt{A/K_1}$ of the hard magnetic environment with the exchange constant A and the first magnetocrystalline anisotropy constant K_1. Otherwise we obtain a strong decrease of the coercivity following a D_{soft}^{-const} law, where D_{soft} is the diameter of the soft magnetic inclusion. According to analytical and numerical investigations, the const varies between -2 and -0.5 depending on the dimension and the geometry of the soft magnetic inclusion. [S0163-1829(98)04517-2]

I. INTRODUCTION

The idea behind composite permanent magnets is the enhancement of the remanence by adding a soft magnetic phase with a high spontaneous polarization to the hard magnetic material. This method is only successful by using special preparation methods like mechanical alloying or rapid solidification. As reported by several authors,[1–11] especially small soft magnetic α-Fe grains of about 10 nm embedded into hard magnetic $Sm_2Fe_{17}N_x$ or $Nd_2Fe_{14}B$ lead to a remarkable remanence enhancement while preserving the coercivity. In order to optimize the magnetic properties, which sensitively depend on the grain structure, a more theoretical understanding of the magnetization processes may be useful. Analytical calculations are generally restricted to simple geometries without taking into account stray-field effects.[12–15] Lee and Chang[16] took stray fields into account, they, however, apply other restrictions which need to be reconsidered. They consider a periodic arrangement of tablet like soft magnetic inclusions within a hard magnetic matrix. The investigation of these authors corresponds to a calculation of the global and local demagnetizing field. The nucleation field is then assumed to be the ideal nucleation field of the curling mode under the action of the calculated demagnetizing field. This is equivalent to a nucleation from the homogeneous state, which is, as the work presented here shows, generally not the case. In many cases not even the remanent state is homogeneous. Furthermore, squareness of the hysteresis loop is assumed and as a consequence nucleation field and coercive field are identical. The work presented here will show that the actual demagnetization process is more complex and the assumption of squareness of the hysteresis loop is not justified. Computational micromagnetism based on the finite element method, allows the rigorous treatment of two- and three-dimensional composite magnets.[17–22] No assumptions on the specific type of magnetization reversal or on the shape of the hysteresis loop are necessary because the magnetization distribution at all fields can be rigorously calculated without any assumptions.

To investigate fundamental magnetization processes in composite materials, we restricted ourselves to a single soft magnetic α-Fe inclusion within a hard magnetic $Nd_2Fe_{14}B$ environment. This paper reveals the conditions on the grain structure, which guarantee an optimal exchange hardening of the α-Fe by taking into account long-range stray-field effects and short-range exchange interactions. Further subjects are the role of the anisotropy, the misorientation, and the shape of the included soft magnetic α-Fe grain for the magnetization reversal process.

II. MICROMAGNETICS

A. General theory

The continuum theory of micromagnetics[23–25] allows the investigation of magnetization processes on length scales greater than atomistic distances and smaller than the macroscopic extension of the magnetic samples. The only prerequisites are information about the magnitude of the measurable material parameters (spontaneous polarization J_s, anisotropy constants K_i, exchange constant A) and details about the microstructure (diameter and geometry of the soft magnetic inclusion). That is sufficient to obtain a stable magnetization distribution by minimizing the total Gibbs free energy

$$\Phi_t[\boldsymbol{J}_s(\gamma_i)]=\int_V\{A[(\nabla\gamma_1)^2+(\nabla\gamma_2)^2+(\nabla\gamma_3)^2] \quad (1)$$

$$+K_1[\gamma_1^2\gamma_2^2+\gamma_2^2\gamma_3^2+\gamma_1^2\gamma_3^2]$$

$$+K_2\gamma_1^2\gamma_2^2\gamma_3^2+\cdots \quad (2)$$

$$-\boldsymbol{J}_s(\gamma_i)\cdot\boldsymbol{H}_{ext} \quad (3)$$

$$-\frac{1}{2}\boldsymbol{J}_s(\gamma_i)\cdot\boldsymbol{H}_s(\gamma_i)\}dV \quad (4)$$

with respect to the direction cosines γ_i $(i=1,2,3)$ of the spontaneous polarization $\boldsymbol{J}_s$ under the restriction $|\boldsymbol{J}_s|=$ const. This constraint is automatically fulfilled by using the polar

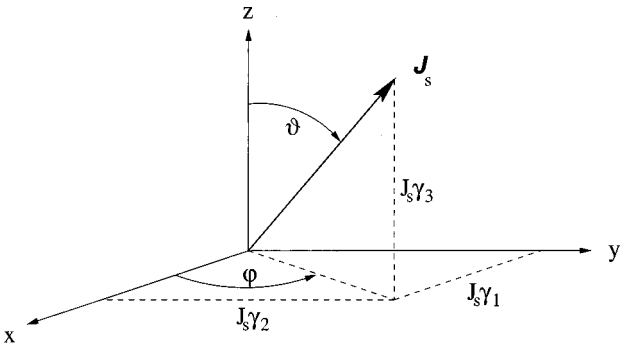

FIG. 1. Definition of the direction cosines $\gamma_1, \gamma_2, \gamma_3$ and spherical coordinates ϑ, φ of the spontaneous polarization $\boldsymbol{J}_s$.

coordinates ϑ and φ defined by Fig. 1. The total energy Φ_t takes into account the short-range exchange interaction of Eq. (1), the anisotropy energy of Eq. (2), the Zeeman contribution of Eq. (3), and the stray-field energy of Eq. (4). The stray field $\boldsymbol{H}_s(\boldsymbol{r})$ can be obtained from Poisson's equation depending on magnetic volume and surface charges.

B. Computational realisation

Since the analytical investigation of different geometries of the soft magnetic inclusion in the presence of all interaction mechanisms is impossible, we developed a numerical algorithm for modeling of composite materials. The discretization of the governing equation for Φ_t is performed by the method of finite elements.[26,27] This allows the investigation of arbitrary shaped grains and therefore the handling of more realistic grain structures. For the minimization of the total Gibbs free energy Φ_t, we use a well-optimized commercial routine based on the so-called ''preconditioned, limited memory quasi-Newton conjugate gradient method.''[28] The long-range stray-field problem is solved by introducing the vector potential $\boldsymbol{A}$ as proposed by Brown.[29] The minimization of the functional

$$W[\boldsymbol{J}_s(\gamma_i),A_x,A_y,A_z]=\int_V\Big\{A[(\nabla\gamma_1)^2+(\nabla\gamma_2)^2+(\nabla\gamma_3)^2]+K_1[\gamma_1^2\gamma_2^2+\gamma_2^2\gamma_3^2+\gamma_1^2\gamma_3^2]+K_2\gamma_1^2\gamma_2^2\gamma_3^2$$
$$+\cdots-\boldsymbol{J}_s(\gamma_i)\cdot\boldsymbol{H}_{ext}-\frac{1}{2\mu_0}[\nabla\times\boldsymbol{A}-\boldsymbol{J}_s(\gamma_i)]^2\Big\}dV \tag{5}$$

with respect to the direction cosine γ_i $(i=1,2,3)$ of the spontaneous polarization and simultaneously to the three components A_x,A_y,A_z of the vector potential $\boldsymbol{A}$ leads to local minima, which are in one-to-one correspondence with those of the total Gibbs free energy Φ_t.[30–32] The Euler-Lagrange equation of Eq. (5) is nothing else than Maxwells equation

$$\nabla\times\boldsymbol{B}(\boldsymbol{r})=\mu_0\boldsymbol{J}_s(\boldsymbol{r}), \tag{6}$$

which connects the stray field $\boldsymbol{B}_s(\boldsymbol{r})=\nabla\times\boldsymbol{A}(\boldsymbol{r})$ with the magnetization distribution $\boldsymbol{J}(\boldsymbol{r})$ and vice versa. For a more detailed description of the simulation model see previous papers.[33,21]

III. EXCHANGE HARDENED AND DECOUPLED SOFT MAGNETIC INCLUSIONS

This section exclusively deals with spherical soft magnetic inclusions embedded into a hard magnetic cube as illustrated by Fig. 2. The edge length of the cube is 150 nm and constant for all following investigations. This guarantees the same reduction of the coercivity due to stray fields of the hard magnetic cube, independently of the diameter and the geometry of the soft magnetic inclusion. The material parameters of $Nd_2Fe_{14}B$ and α-Fe are summarized by Table I at room temperature.

A. Demagnetization curves for different diameters of the soft magnetic sphere

To prepare composite magnets with a sufficiently high coercivity, the soft magnetic grains must be exchange hard-

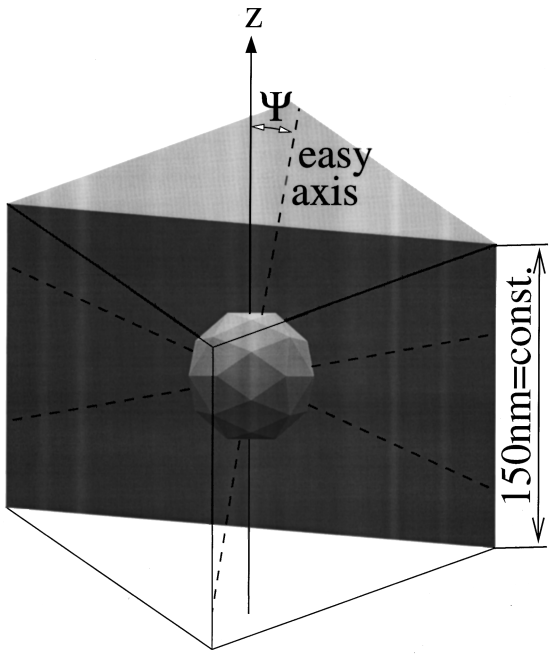

FIG. 2. Simple model of composite permanent magnet, which consists of a quasispherical α-Fe inclusion within a hard magnetic $Nd_2Fe_{14}B$ cube. The angle Ψ_0 between the easy axes of the α-Fe (cubic anisotropy) and the z axis is the misorientation of the soft magnetic sphere. The easy axis of the hard magnetic environment (uniaxial anisotropy) is parallel to the z axis, which is identical with the direction of the applied field.

TABLE I. Spontaneous polarization J_s, anisotropy constants K_i, exchange constant A, and width of the Bloch wall $\delta_B = \pi\sqrt{A/K_1}$ at $T = 300$ K for hard magnetic $Nd_2Fe_{14}B$ and soft magnetic α-Fe.

Material	J_s (T)	K_1 (10^6 J/m^3)	K_2 (10^6 J/m^3)	$A(10^{-12}$ J/m)	δ_B (nm)	Ref.
$Nd_2Fe_{14}B$	1.61	4.331	0.6491	7.7	4.2	37
α-Fe	2.15	0.046	0.015	25.0	73.2	38

ened by their hard magnetic environment. Because of the limited range of the exchange interaction of about $\delta_B \approx 5$ nm, the spatial extension of the soft magnetic inclusion plays a decisive role. So we calculated the demagnetization curves of the magnetic structure of Fig. 2 for different diameters of the soft magnetic sphere. Figure 3 shows the results for D_{sphere} between 10 and 120 nm. Characteristic is the loss of the rectangularity of the demagnetization curves with increasing diameter of the sphere, which can be attributed to the failure of the exchange hardening of the soft magnetic region.

B. Remanence as a function of the diameter of the soft magnetic sphere

Figure 4 shows the computed remanence J_r as a function of the diameter of the sphere D_{sphere}, which is approximately given by

$$J_r = J_{sat} = v_{soft} J_s^{soft} + v_{hard} J_s^{hard}$$
$$= v_{soft}\ 2.15\ \text{T} + (1 - v_{soft})\ 1.16\ \text{T}$$
$$\text{for}\ D_{sphere} \leqslant 90\ \text{nm}, \qquad (7)$$

where $v_{soft} = V_{soft}/V_{total}$ denotes the fraction of α-Fe ($V_{soft} = \pi D_{sphere}^3/6$) relative to the total magnet ($V_{total} = 150^3$ nm^3). For diameters of the sphere smaller than 90 nm, the short-range exchange interaction dominates and preserves the uniform magnetization distribution. But for spheres greater than 90 nm, the long-range stray field destroys the parallel alignment of the soft magnetic moments and creates magnetic vortices. This is demonstrated in Fig. 5 for $D_{sphere} = 100$ and 120 nm for the remanent states. If the numerical algorithm does not take into account long-range stray fields, the vortex states vanish.

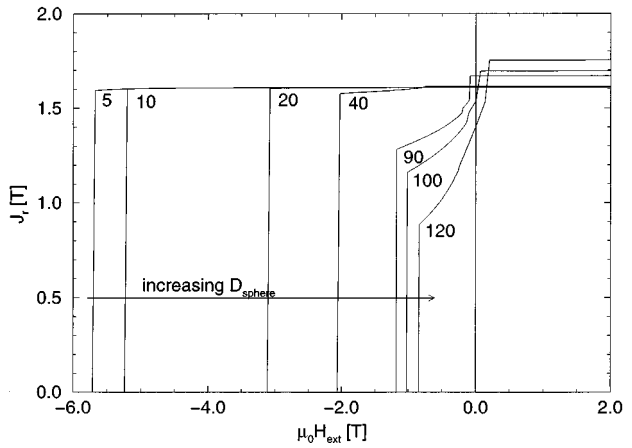

FIG. 3. Computed demagnetization curves for the magnetic structure of Fig. 2 with increasing diameter D_{sphere} (nm) of the soft magnetic sphere.

C. Coercivity as a function of the diameter of the soft magnetic sphere

Figure 6 shows the computed coercivity H_c as a function of the diameter of the soft magnetic sphere D_{sphere}. In presence of an opposite field, the exchange hardening of the soft magnetic inclusion can only be guaranteed for diameters smaller than 10 nm. Therefore the characteristic range of the exchange interaction is in order of $2\delta_B^{hard}$. For greater spheres, the coercivity decreases according to following analytical expression:

$$H_c \sim D_{sphere}^{-0.701} \quad \text{for}\ D_{sphere} > 10\ \text{nm}. \qquad (8)$$

Note the strong reduction of the coercivity for $D_{sphere} > 10$ nm, where the exchange hardening begins to fail.

D. Discussion of the magnetization reversal processes

The plots of the magnetization vectors of Figs. 7, 8, and 9 for $D_{sphere} = 20$,90, and 100 nm are useful to improve the understanding of the demagnetization processes for composite materials. For $D_{sphere} = 10$ nm, the soft magnetic moments are ideally exchange coupled by the hard magnetic environ-

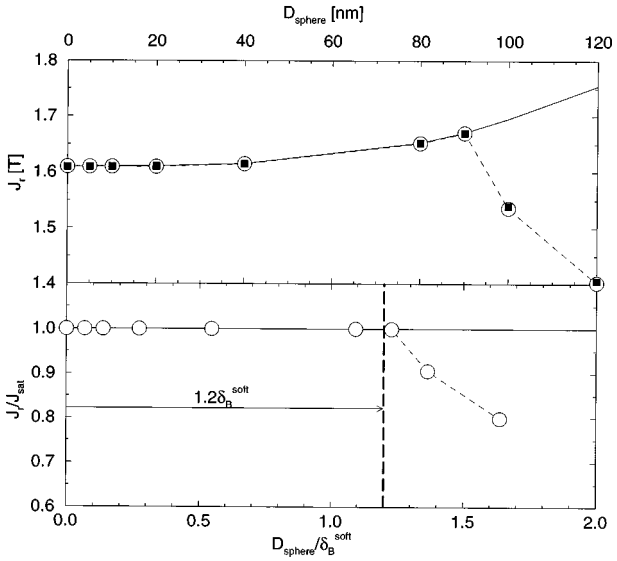

FIG. 4. Computed remanence J_r (and J_r/J_{sat}) as a function of the diameter D_{sphere} (and $D_{sphere}/\delta_B^{soft}$) of the soft magnetic sphere. J_{sat} denotes the saturation polarization defined by Eq. (7). δ_B^{soft} is the width of the Bloch wall given by Table I for the soft magnetic phase. The opaque circles belong to an ideal oriented sphere with $\Psi_0 = 0°$ and the filled squares to a misorientation of $\Psi_0 = 45°$.

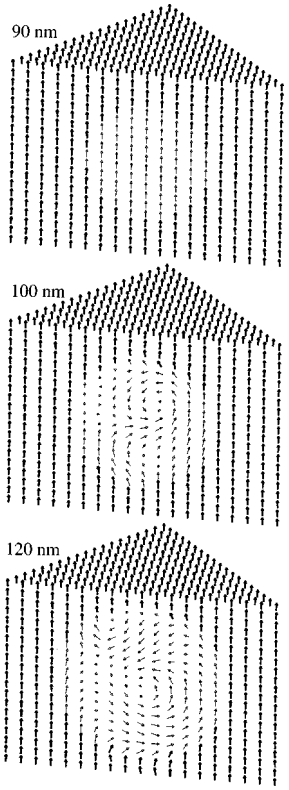

FIG. 5. Vector plots of the magnetization at the remanent states with increasing diameter of the soft magnetic sphere (thin arrows): $D_{\text{sphere}}=90$, 100, and 120 nm. For $D_{\text{sphere}}>90$ nm the magnetization distribution is no longer determined by the short-range exchange interaction. The magnetic vortex structures result from long-range strayfields.

ment. All magnetic moments reverse their directions spontaneously and uniformly at $0.77H_{\text{N}}^{(0)}$. The reduction with respect to the ideal nucleation field $H_{\text{N}}^{(0)}=2K_1/J_{\text{s}}$ for an ideal Stoner-Wohlfahrt particle can be entirely attributed to nonuniform stray fields of the hard magnetic cube.[34] For $D_{\text{sphere}}=20$ nm (see Fig. 7), the magnetization reversal is nucleated by the soft magnetic inclusion. At the overcritical state, just before magnetization reversal, the soft magnetic moments turn out of their easy axis more in opposite field direction. The hard magnetic moments deviate from their easy axis, as well, within $\delta_{\text{B}}^{\text{hard}}\approx 5$ nm around the soft magnetic sphere. For $D_{\text{sphere}}=90$ nm (see Fig. 8), the exchange hardening of the soft magnetic region is still guaranteed for the remanent state. But even a small opposite field of only about $0.014H_{\text{N}}^{(0)}$ leads to two magnetic vortices, which can be considered a stray field effect. With increasing opposite field the region with reversed soft magnetic moments grows and the two vortices shift near the surface of the sphere. For $D_{\text{sphere}}=120$ nm (see Fig. 9), there already exist vortex structures for positive applied fields of about $0.002H_{\text{N}}^{(0)}$. Contrary to the previous case of $D_{\text{sphere}}=90$ nm, we obtain only one vortex at the remanent state. At the overcritical state, most of the soft magnetic moments are reversed. Only within a small region of about $\delta_{\text{B}}^{\text{hard}}\approx 5$ nm, is the magnetization distribution still influenced by the exchange interaction. The transitions between the soft and hard magnetic region are a complex composition of different wall types.[35]

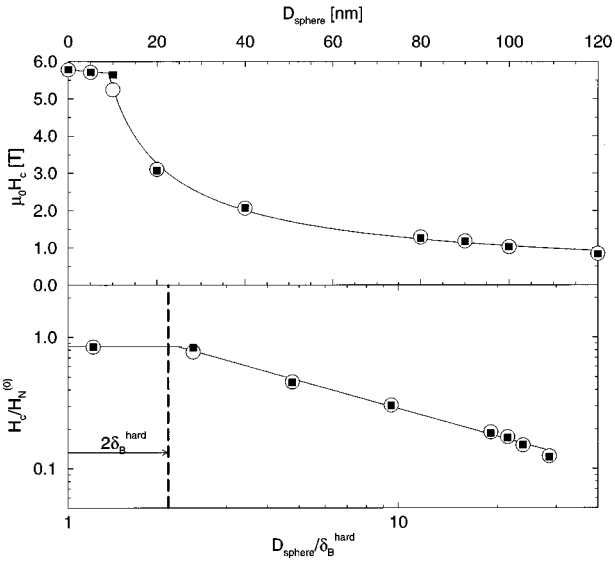

FIG. 6. Computed coercivity $\mu_0 H_{\text{c}}$ (and $H_{\text{c}}/H_{\text{N}}^{(0)}$) as a function of the diameter D_{sphere} (and $D_{\text{sphere}}/\delta_{\text{B}}^{\text{hard}}$) of the soft magnetic sphere illustrated by Fig. 2. $H_{\text{N}}^{(0)}$ is the ideal nucleation field $2K_1/J_s$ for an ideal Stoner-Wohlfarth particle. And δ_B^{hard} denotes the width of the Bloch wall given by Table I for the hard magnetic phase. The opaque circles belong to an ideal oriented sphere with $\Psi_0=0°$ and the filled squares to a misorientation of $\Psi_0=45°$.

E. The role of cubic anisotropy of α-Fe in composite magnets

Figures 4 and 6 show the computed remanence and coercivity by using the exact cubic anisotropy of α-Fe by opaque circles. But approximately the same results are obtained by assuming an uniaxial anisotropy (see filled squares). So we can conclude that the type of the anisotropy of α-Fe plays only a minor role during the magnetization reversal process for composite materials. More important is the relative strength between the short-range exchange and the long-range dipole-dipole interaction within the soft magnetic region.

F. The role of the misorientation of α-Fe in composite magnets

Because of the small anisotropy of α-Fe, the misorientation Ψ, defined in Fig. 2 as the angle between the easy axis and the z axis, does not effect the magnetization reversal process. According to Fig. 10, the remanence and also the coercivity are independent of the misorientation Ψ. For $D_{\text{sphere}}=10$ nm, the exchange hardening of the soft magnetic moments by the hard magnetic environment dominates. And for $D_{\text{sphere}}=120$ nm, the stray field mainly determines the directions of the soft magnetic moments. Therefore the anisotropy of soft magnetic grains in composite magnets can be neglected in all cases.

IV. EFFECT OF THE GEOMETRY OF THE SOFT MAGNETIC INCLUSION

A. Soft magnetic cube

For the optimization of high-remanent composite magnets, the volume fraction of the exchange hardened soft magnetic phase should be maximized. This maximum soft mag-

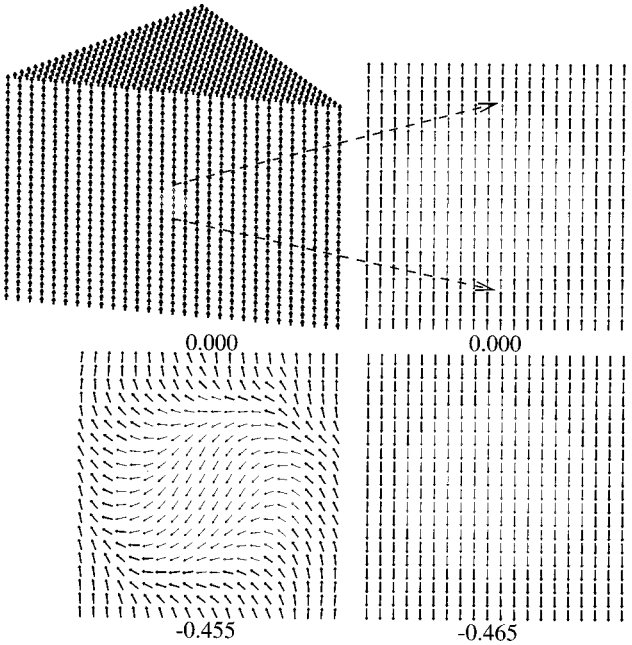

FIG. 7. Computed magnetization reversal process for the magnetic structure of Fig. 2 for $D_{\text{sphere}}=20$ nm. The numbers are the external fields in units of the ideal nucleation field $H_{\text{N}}^{(0)}$ of the hard magnetic phase. The thin (thick) arrows belong to the hard magnetic (soft magnetic) regions.

netic volume depends on the shape of the soft magnetic grains embedded into the hard magnetic environment.

According to Figs. 11 and 12, we obtain the following relations for the remanence J_{r} and the coercivity H_c of the soft magnetic cube embedded into the hard magnetic environment:

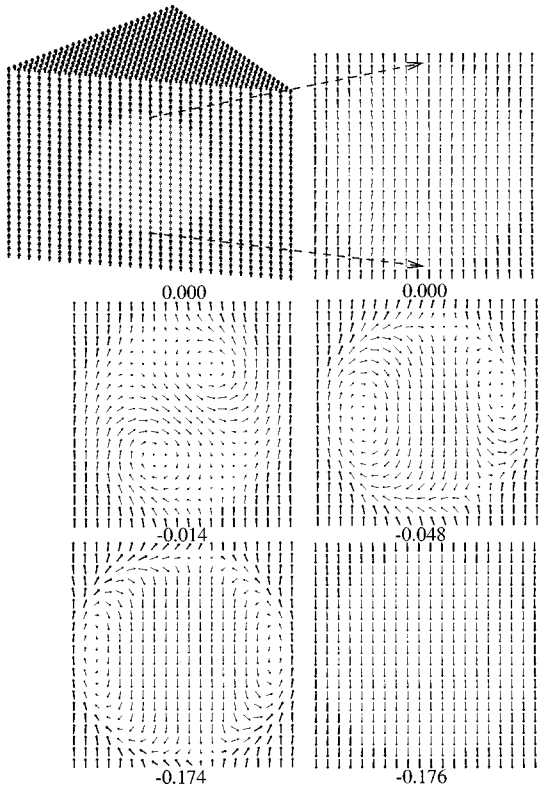

FIG. 8. See caption of Fig. 7, but now for $D_{\text{sphere}}=90$ nm.

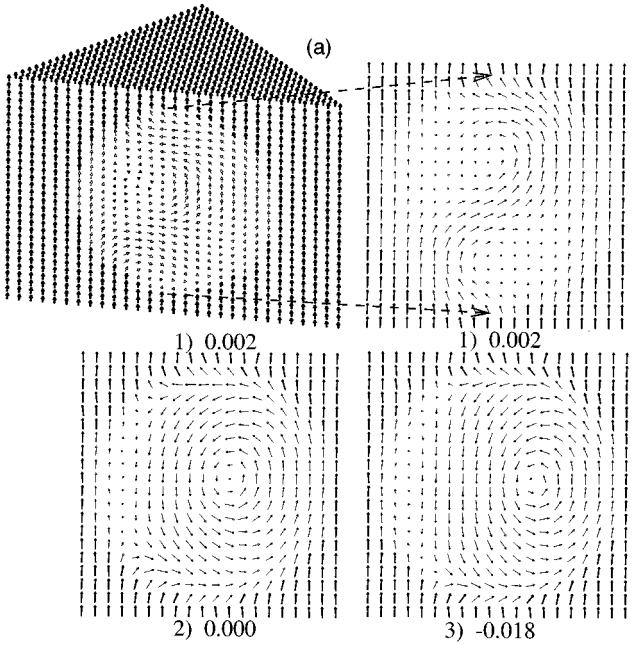

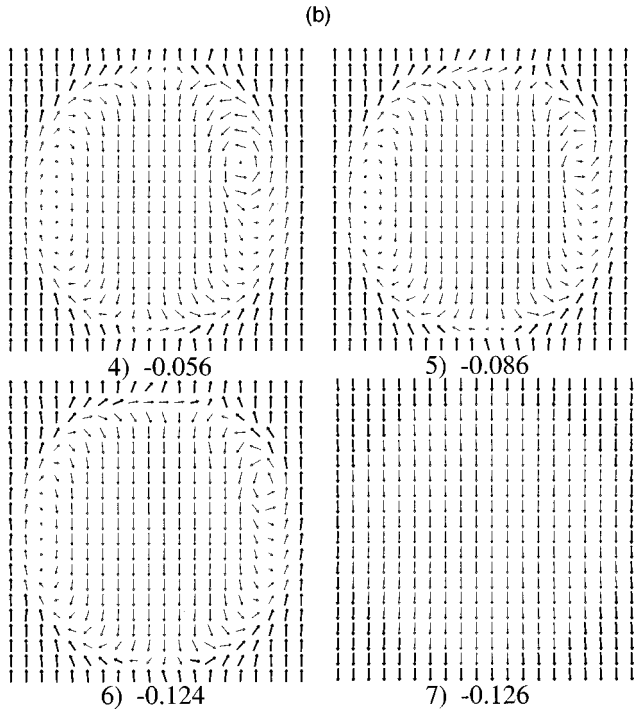

FIG. 9. See caption of Fig. 7, but now for $D_{\text{sphere}}=120$ nm.

$$J_{\text{r}}=v_{\text{soft}}J_{\text{s}}^{\text{soft}}+v_{\text{hard}}J_{\text{s}}^{\text{hard}}v_{\text{soft}}2.15\text{T}+(1-v_{\text{soft}})1.61\text{T} \quad \text{for } \langle D\rangle\leqslant 110 \text{ nm}, \tag{9}$$

$$H_{\text{c}}\sim\langle D\rangle^{-0.762} \quad \text{for } \langle D\rangle\geqslant 15 \text{ nm}. \tag{10}$$

The quantity $\langle D\rangle=(6V_{\text{soft}}/\pi)^{1/3}$ denotes the diameter of a fictitious sphere with the volume $V_{\text{soft}}=L_{\text{soft}}^3$ of the soft magnetic cube. Analogous to Eq. (7) $v_{\text{soft}}=V_{\text{soft}}/V_{\text{total}}$ defines the volume fraction of the α-Fe cube relative to the total magnet.

By comparing Eqs. (7) and (9) or the circles and squares of Fig. 11, the exchange hardening of the soft magnetic inclusion at the remanent state is guaranteed within $D_{\text{sphere}}\leqslant 90$ nm$\approx 1.2\delta_{\text{B}}^{\text{soft}}$ for the sphere and $\langle D\rangle\leqslant 110$ nm

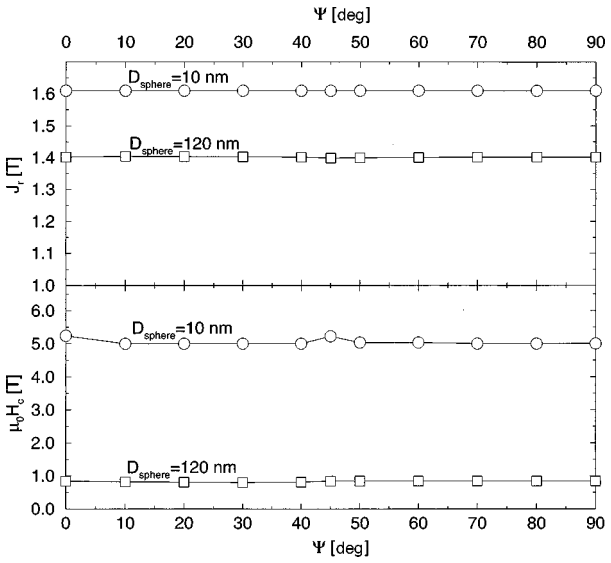

FIG. 10. Remanence J_r and coercivity $\mu_0 H_c$ as a function of the misorientation Ψ of the soft magnetic sphere. Independent of the diameter of the soft magnetic sphere, the remanence and coercivity do not change significantly with varying misorientation.

$\approx 1.5\delta_B^{soft}$ for the cube. Obviously larger soft magnetic volumes can be exchange coupled by cubic than by spherical inclusions. Also in the presence of opposite applied fields, the exchange hardening seems to be more effective for the cubic inclusion. By comparing Eqs. (8) and (10) or the circles and squares of Fig. 12, the coercivity approximately keeps constant within $D_{sphere} \leqslant 10$ nm$\approx 2\delta_B^{hard}$ for the sphere and $\langle D \rangle \leqslant 15$ nm$\approx 3\delta_B^{hard}$ for the cube. The origin of this behavior is illustrated in Fig. 13. Important for the exchange hardening is only the range of the exchange interaction, which is approximately determined by the width δ_B of the

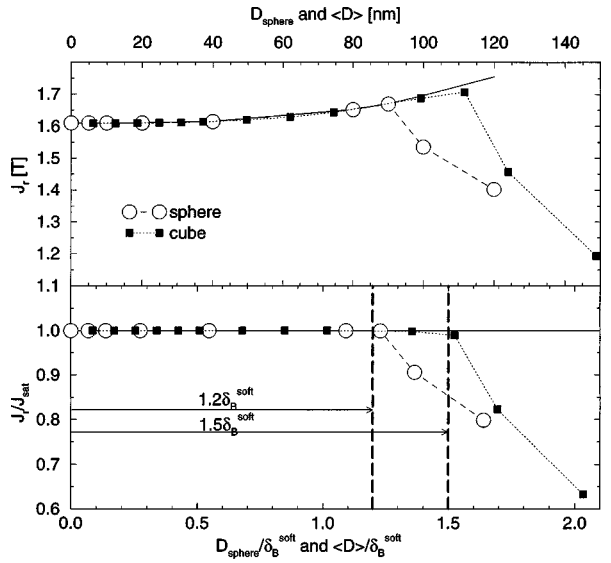

FIG. 11. Computed remanence J_r (and J_r/J_{sat}) as a function of the diameter D_{sphere} or $\langle D \rangle$ (and $D_{sphere}/\delta_B^{soft}$ or $\langle D \rangle/\delta_B^{hard}$) of the soft magnetic sphere or cube. J_{sat} denotes the saturation polarization defined by Eq. (7). δ_B^{soft} is the width of the Bloch wall tabled in Table I for the soft magnetic phase. Finally $\langle D \rangle$ is calculated by $(6V_{soft}/\pi)^{1/6}$, where $V_{soft}=L_{cube}^3$.

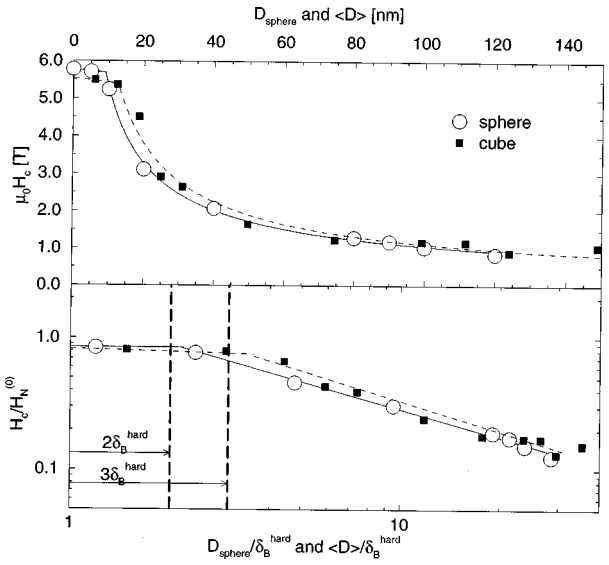

FIG. 12. Computed coercivity $\mu_0 H_c$ (and $H_c/H_N^{(0)}$) as a function of the diameter D_{sphere} or $\langle D \rangle$ (and $D_{sphere}/\delta_B^{hard}$ or $\langle D \rangle/\delta_B^{hard}$) of the soft magnetic sphere or cube. $H_N^{(0)}$ is the ideal nucleation field $2K_1/J_s$ for an ideal Stoner-Wohlfarth particle. And δ_B^{hard} denotes the width of the Bloch wall shown in Table I for the hard magnetic phase. Finally $\langle D \rangle$ is calculated by $(6V_{soft}/\pi)^{1/6}$, where $V_{soft}=L_{cube}^3$ results from the edge length L_{cube} of the cube.

Bloch wall. In addition to the sphere, the shaded regions of the cube are also well exchange coupled. So a larger soft magnetic volume can be exchange coupled by cubic than by spherical inclusions.

If the exchange hardening begins to fail with increasing extension of the soft magnetic inclusions, Figs. 11 and 12 show a stronger reduction of the remanence and coercivity for the cube than for the sphere. This effect may be attributed to large local stray fields near the sharp edges and corners of the cube. Local stray fields lead to strongly nonuniform magnetization distributions and therefore assist the magnetization reversal.

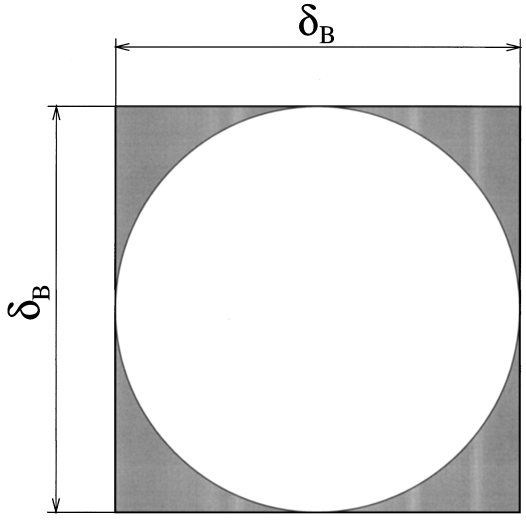

FIG. 13. The complete exchange hardened region is greater for the soft magnetic cube than for the sphere. The difference is indicated by the shaded regions.

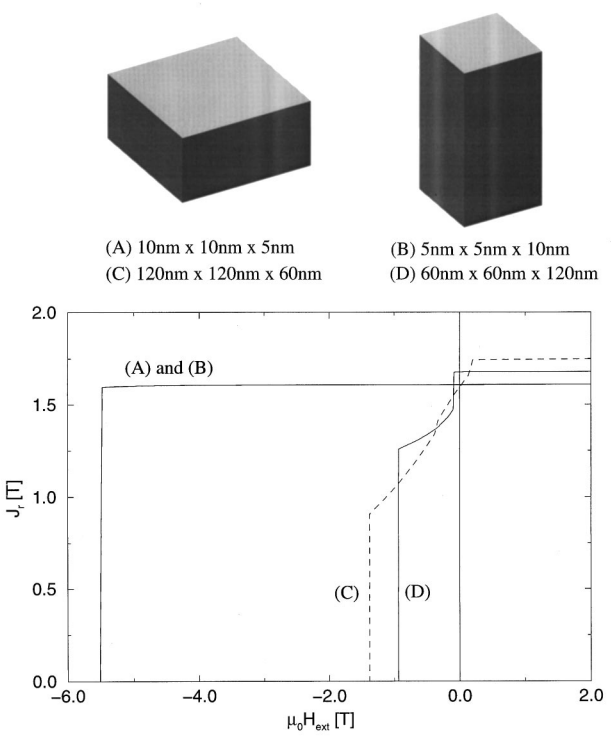

FIG. 14. Top: soft magnetic plate (left) and prism (right) placed in the center of the hard magnetic cube with an edge length of 150 nm. Bottom: corresponding demagnetization curves.

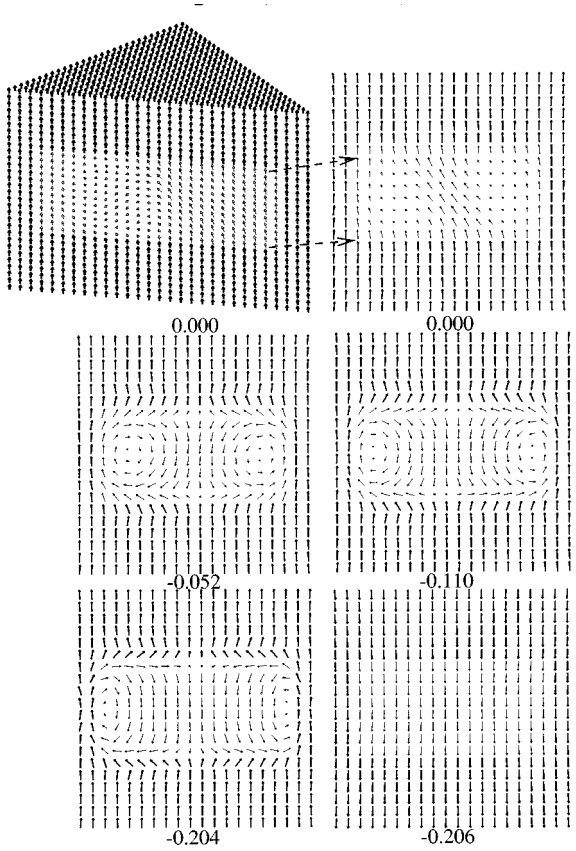

FIG. 15. Computed magnetization reversal process for the plate C presented by Fig. 14. The strong (thin) arrows belong to the hard- (soft-) magnetic phase. The numbers are the values of the applied fields in units of the ideal nucleation field $H_N^{(0)}$ of the hard magnetic phase. The vortex states can be attributed to local stray fields.

B. Soft magnetic plates and rectangular prisms

Figure 14 shows the investigated soft magnetic inclusions and the corresponding demagnetization curves. If one edge length is of about $\delta_B^{hard} \approx 5$ nm, the soft magnetic region is ideally exchange coupled by the hard magnetic environment. Therefore the demagnetization process does not significantly depend on the shape of the included soft magnetic grain. According to Fig. 14, the demagnetization curves of the inclusions A (10 nm$\times$10 nm$\times$5 nm) and B (5 nm $\times$5 nm$\times$10 nm) are identical. But if the smallest edge length of the embedded grain is greater than $\delta_B^{hard} \approx 5$ nm, the complete exchange hardening of all soft magnetic moments begins to fail. In this case, the magnetization reversal process depends on local stray fields and therefore on the concrete shape of the soft magnetic grain as shown by the demagnetization curves C (120 nm$\times$120 nm$\times$60 nm) and D (60 nm$\times$60 nm$\times$120 nm) of Fig. 14. According to Fig. 15, the energetically lowest state is obtained by creating two vortices. This magnetization distribution minimizes the stray field energy and keeps the exchange energy sufficiently low. Only within small regions does there exist 180° domain walls between the hard and soft magnetic phase. The creation of vortices within the soft magnetic rectangular prism is more difficult, as illustrated by Fig. 16. Furthermore, there exist large regions between the soft and hard magnetic grain boundary with 180° domain walls (see especially Fig. 16 for $0.052 H_N^{(0)}$). So we can conclude that soft magnetic prisms lead to greater stray-field and exchange energies than soft magnetic plates. This explains the smaller coercivity of the prism compared to the plate, as presented by the demagnetization curves C and D of Fig. 14.

V. COMPARISION WITH ANALYTICAL CALCULATIONS

A simple model of a soft magnetic inclusion in a hard magnetic surrounding is a thin α-Fe layer which is enclosed by two $Nd_2Fe_{14}B$ bulks spreading to infinity as shown by Fig. 17. Applying a few justifiable approximations, the macroscopic magnetic properties of this model magnet can be calculated analytically within the theory of micromagnetics.[14] The energy contributions to the Gibbs free energy taken into account are the magnetocrystalline, the exchange, and the Zeeman energy for the hard magnetic bulks, in the soft layer the magnetocrystalline energy is negligible since it is two orders of magnitude smaller than in the hard magnetic regions. We only consider in-plane distributions of the magnetic moments corresponding to Bloch-wall-type configurations. This guarantees a vanishing stray field. The variation of the Gibbs energy now leads to the well-known Euler-Lagrange differential equation for the polar angle $\vartheta \equiv \vartheta(x)$ of the orientation of magnetic moments throughout the magnetic material. The polar angle as used here is defined by Figs. 1 and 17 and as the angle enclosed between the magnetization and the z axis. According to Leineweber and Kronmüller,[14] the explicit solution for the orientation of polarization reads

$$\vartheta(x)=\begin{cases} 2\cdot\arctan\left(\tan\dfrac{\vartheta_0}{2}\cdot\mathrm{cn}\left[k;\dfrac{x}{\delta_B^{soft}}\sqrt{-h_{ext}\dfrac{K_1^{hard}J_s^{soft}}{K_1^{soft}J_s^{hard}}}\right]\right) & \text{for} \quad x\leqslant\dfrac{D_{soft}}{2},\\ 2\cdot\mathrm{arccot}\left(\sqrt{\dfrac{-h_{ext}}{1+h_{ext}}}\cosh[X]\right) & \text{for} \quad x>\dfrac{D_{soft}}{2},\end{cases}$$

$$X=\frac{x-D_{soft}/2}{\delta_B^{hard}}\sqrt{1+h_{ext}}+\mathrm{arcosh}\left(\frac{\cot(\vartheta_d/2)}{\sqrt{-h_{ext}/(1+h_{ext})}}\right). \tag{11}$$

The center of the soft layer is located at $x=0$, the boundary between the regions at $x=\pm D_{soft}/2$. The angles $\vartheta_0\equiv\vartheta(x=0)$ and $\vartheta_d\equiv\vartheta(x=\pm D_{soft}/2)$ denote the orientation of the polarization in the layer center and in the boundary between regions, respectively. The superscripts soft and hard refer to the soft α-Fe and the hard $Nd_2Fe_{14}B$, J_s is the spontaneous polarization of the respective material, K_1 is the first anisotropy constant, and δ_B the Bloch wall width defined as $\pi\sqrt{A/K_1}$ with the exchange constant A. The applied field is denoted by h_{ext}, which is defined as the applied field in units of the ideal nucleation field $H_N^{(0)}$ of the hard magnetic component ($h_{ext}\equiv H_{ext}/H_N^{(0)}$ and $H_N^{(0)}=2K_1/J_s$). The function $\mathrm{cn}[k;\varphi]$ denotes the cosine amplitude of the elliptic integral of the first kind,[36] its modulus k in the given case reads: $k=\sin(\vartheta_0/2)$.

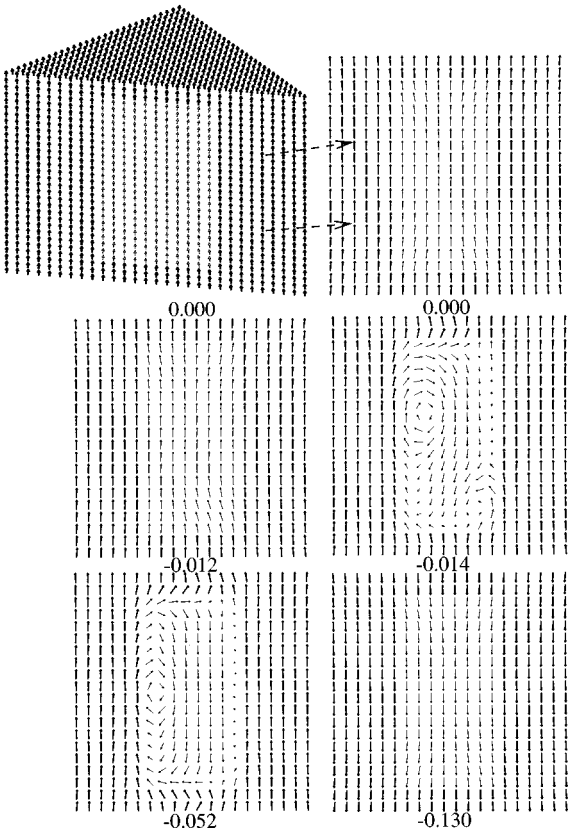

FIG. 16. See caption of Fig. 15. But now for the prism D presented by Fig. 14. The importance of stray fields in soft magnetic regions shows the vector plot for $H_{ext}=0$. The soft magnetic moments near the corners of the prism deviates stronger from the $+z$ direction than the hard magnetic ones.

Unfortunately it is not possible to deduce an explicit expression for the coercivity. Investigation of the stability of the solution of Eq. (11), however, yields the coercivity for each given thickness of the soft layer D_{soft}. Figure 18 shows the results of this investigation by opaque squares. For soft magnetic layers thinner than approximately the hard magnetic Bloch wall thickness, the coercivity proves to be identical with the ideal hard magnetic nucleation field $H_N^{(0)}=2K_1/J_s=6.71$ T. The magnetization reversal mode is rotation in unison just as in an ideal homogeneous hard magnetic material. For intermediate layer thicknesses $\delta_B^{hard}<D_{soft}<8\,\delta_B^{hard}$, the coercivity rapidly decreases with the soft layer thickness. Magnetization reversal is nucleated by uniform rotation of the soft magnetic moments according to Stoner and Wohlfahrt and then spreads throughout the whole magnet. For even thicker soft layers, the coercivity decreases with an inverse power of the thickness of the soft layers. Here magnetization reversal in the soft layer is complete before, at higher fields, magnetization reversal in the hard magnetic regions sets in. Thus we can summarize:

$$H_c(D^{soft})=\begin{cases} H_N^{(0)}(\text{hard magnetic}) & \text{for} \quad D_{soft}\leqslant\delta_B^{hard}\\ \text{rapid decrease} & \text{for} \quad \delta_B^{hard}<D_{soft}<8\,\delta_B^{hard}\\ \sim D_{soft}^{-1.75} & \text{for} \quad D_{soft}>8\,\delta_B^{hard}.\end{cases} \tag{12}$$

Figure 18 additionally compares the analytical results for multilayers with numerical dates for a spherical inclusion. The differences may be attributed to the different dimensions of the respective soft magnetic inclusions. But for $D_{soft}>8\,\delta_B^{hard}$ both calculations lead to a decrease of the coercivity following an inverse power law. Further investigation yields that these results remain qualitatively the same under variation of the material parameters. Especially the value of the exponent in the observed decrease of the coercivity with the layer thickness proves to be almost independent of the specific material parameters. This result implies that the decrease of the coercivity in an inverse power law is a consequence of the failure of the exchange interaction to harden the soft magnetic layer. If we take the hard magnetic Bloch wall thickness δ_B^{hard} as a measure of how deep the exchange interaction can propagate from the hard regions into the soft region, then the coercivity will only depend on the ratio of

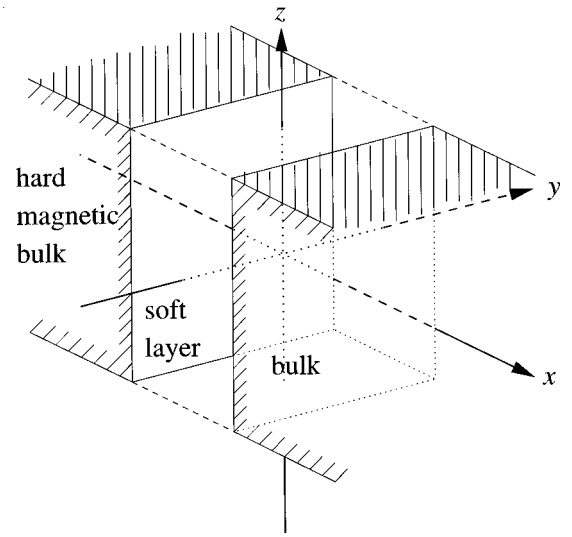

FIG. 17. Model for a composite magnet; a magnetically soft layer enclosed by a hard magnetic material. Both the layer and the bulk are assumed to spread to infinity in the z and y directions, the layer is limited to $-D_{\mathrm{soft}}/2<x<D_{\mathrm{soft}}/2$.

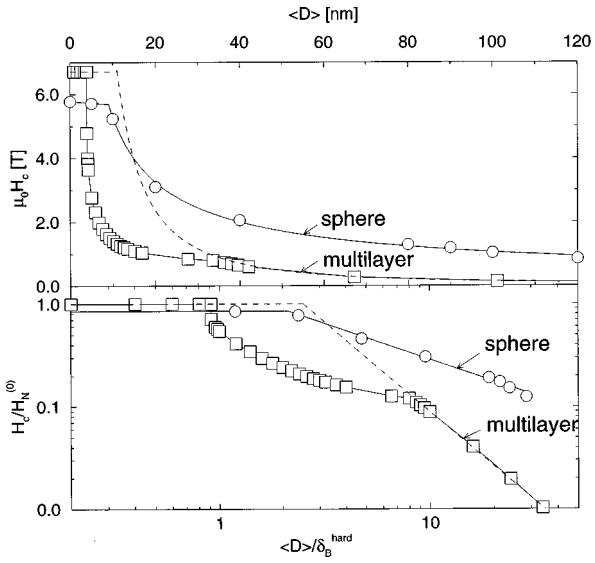

FIG. 18. Coercivity of multilayers and spheres in comparision. For the α-Fe/$Nd_2Fe_{14}B$ multilayer $\langle D\rangle$ equals the thickness D_{soft} of the α-Fe layers. For the spherical α-Fe inclusion embedded within an $Nd_2Fe_{14}B$ cube $\langle D\rangle$ equals the diameter D_{sphere} of the α-Fe sphere. For $D_{\mathrm{soft}}\geqslant 8\,\delta_B^{\mathrm{hard}}$ the analytical result for multilayers is qualitatively similar to the numerical result of the soft magnetic sphere. The differences for $D_{\mathrm{soft}}<8\,\delta_B^{\mathrm{hard}}$ may be attributed to the dimension of the problems (one-dimensional for soft magnetic multilayers and three-dimensional for the soft magnetic sphere).

layer thickness to hard magnetic exchange length, not on their absolute values. If this interpretation is correct, the exponent of the inverse power-law decrease will strongly depend on the geometry of the soft inclusion. Depending on the ratio of surface to volume of the soft inclusion, the exchange interaction propagating from the hard magnetic surrounding can reach a different volume fraction of the soft inclusion, thus the exchange hardening will be more or less effective.

VI. CONCLUSION

The magnetization reversal of nanoscaled composite magnets is mainly determined by short-range exchange and long-range dipole-dipole interactions. Details about the magnetocrystalline anisotropy of the soft magnetic phase have no effect. The exchange interaction induces magnetic hardness into the soft magnetic phase and the dipole-dipole interaction creates magnetic vortex structures within the soft magnetic region. Depending on the extension of the soft magnetic inclusion, the exchange or dipole-dipole interaction finally dominates and determines the magnetization reversal process. The characteristic range of the exchange interaction is given by the width of the Bloch wall

$$\delta_B=\pi\sqrt{\frac{A}{K_1}}. \tag{13}$$

Therefore the largest extension of the soft magnetic inclusions should be smaller than twice the domain-wall width of Eq. (13) to guarantee an optimal exchange hardening and to suppress vortex states by local stray fields.

The maximum remanence of composite magnets can be obtained, if the nucleation of the soft magnetic moments is avoided for positive applied external fields $H_{\mathrm{ext}}\geqslant 0$. So the largest extension D_{soft} of the soft magnetic inclusion should be smaller than twice the domain-wall width $2\,\delta_B^{\mathrm{soft}}$ and therefore smaller than 140 nm for $Nd_2Fe_{14}B$ at $T=300$ K. In fact local stray fields reduce this maximum extension to approximately one Bloch wall width

$$D_{\mathrm{soft}}\leqslant\delta_B^{\mathrm{soft}}\approx 70\ \ \mathrm{nm}\quad (H_{\mathrm{ext}}\geqslant 0) \tag{14}$$

for $Nd_2Fe_{14}B$ at $T=300$ K. The maximum coercivity of composite magnets can be only guaranteed by suppressing the magnetization reversal of the hard magnetic environment induced by the reversed soft magnetic moments. So the largest extension D_{soft} of the soft magnetic inclusion should be smaller than twice the domain-wall width

$$D_{\mathrm{soft}}\leqslant 2\,\delta_B^{\mathrm{hard}}\approx 10\ \ \mathrm{nm}\quad (H_{\mathrm{ext}}\approx H_c) \tag{15}$$

for $Nd_2Fe_{14}B$ at $T=300$ K. Therefore the optimized grain structure of composite magnets consists of soft magnetic grains smaller than $2\,\delta_B^{\mathrm{hard}}$ embedded into the hard magnetic environment.

Both analytical and numerical calculations reveal that for larger soft magnetic inclusions, a decrease of the coercivity with an inverse power of the diameter of the inclusion is observed:

$$H_c\sim D_{\mathrm{soft}}^{-\mathrm{const}}\quad \text{for}\quad D>2\,\delta_B^{\mathrm{hard}}. \tag{16}$$

The exponent of the power-law decrease is found to depend on the geometry of the soft magnetic inclusion:

$$\text{const} = \begin{cases} 1.750 & \text{for multilayers (one-dimensional),} \\ 0.762 & \text{for cubic inclusions (three-dimensional),} \\ 0.701 & \text{for spherical inclusions (three-dimensional).} \end{cases} \tag{17}$$

As a reason for this behavior, we suggest the different surface to volume ratios for each specific geometry of the inclusion. Depending on this ratio, a different volume fraction of the soft magnetic inclusion can be exchange hardened by the exchange interaction which is propagating from the surface of the inclusion into its volume. Apart from the influence on the exchange hardening, the geometry of the soft magnetic inclusion determines the local demagnetization field. Inclusions with edges and corners have a much higher and more inhomogeneous demagnetization field than a spheric inclusion. This demagnetization field decreases the coercivity even further.

[1] J. Ding, P. G. McCormick, and R. Street, J. Magn. Magn. Mater. **124**, 1 (1993).

[2] J. Ding, P. McCormick, and R. Street, in *8th International Symposium on Magnetic Anisotropy and Coercivity in Rare Earth-Transition Metal alloys, Birmingham, Sept. 15, 1994*, edited by C. Manwaring, D. Jones, A. Williams, and I. Harris (The University of Birmingham, Edgbaston, Birmingham, United Kingdom, 1994), pp. 63–70.

[3] J. Ding, Y. Liu, R. Street, and P. McCormick, J. Appl. Phys. **75**, 1032 (1994).

[4] P. McCormick, J. Ding, Y. Liu, and R. Street, in *Proceedings of the 2nd International Conference on Structural Applications of Mechanical Alloying*, edited by J. deBarbadillo, F. Fores, and R. Schwarz (ASM, Materials Park, Ohio, University Western Australia, Nedlands, Australia, 1993), Vol. 2, pp. 349–352.

[5] A. Manaf, R. A. Buckley, H. A. Davies, and M. Leonowicz, J. Magn. Magn. Mater. **128**, 302 (1993).

[6] A. Manaf, M. Al-Khafaji, P. Zhang, H. Davies, R. Buckley, and W. Rainforth, J. Magn. Magn. Mater. **128**, 307 (1993).

[7] A. Manaf, P. Zhang, I. Ahmed, H. Davies, and R. Buckley, IEEE Trans. Magn. **29**, 2866 (1993).

[8] P. Zhang, M. Al-Khafaji, R. Buckley, W. Rainforth, and H. Davies, in *8th International Symposium on Magnetic Anisotropy and Coercivity in Rare Earth-Transition Metal alloys, Birmingham, Sept. 15, 1994* (Ref. 2), pp. 249–255.

[9] M. Willcox, J. Williams, M. Leonowicz, A. Manaf, and H. Davies, in *8th International Symposium on Magnetic Anisotropy and Coercivity in Rare Earth-Transition Metal alloys, Birmingham, Sept. 15, 1994* (Ref. 2), pp. 443–453.

[10] S. Hirosawa and H. Kanekiyo, in *8th International Symposium on Magnetic Anisotropy and Coercivity in Rare Earth-Transition Metal alloys, Birmingham, Sept. 15, 1994* (Ref. 2), pp. 87–94.

[11] J. Fidler, K. G. Knoch, H. Kronmüller, and G. Schneider, J. Mater. Res. **4**, 806 (1989).

[12] R. Coehoorn, D. B. Mooij, and C. D. E. Waard, J. Magn. Magn. Mater. **80**, 101 (1989).

[13] R. Skomski and J. M. D. Coey, IEEE Trans. Magn. **29**, 2860 (1993).

[14] T. Leineweber and H. Kronmüller, J. Magn. Magn. Mater. (to be published 1997).

[15] T. Leineweber and H. Kronmüller, Phys. Status Solidi B **201**, 291 (1997).

[16] C.-M. Lee and C.-R. Chang, J. Appl. Phys. **79**, 4462 (1996).

[17] E. Feutrill, P. McCormick, P. Smith, and R. Street, in *8th International Symposium on Magnetic Anisotropy and Coercivity in Rare Earth-Transition Metal alloys, Birmingham, Sept. 15, 1994* (Ref. 2), pp. 279–305.

[18] T. Schrefl, H. Kronmüller, and J. Fidler, J. Magn. Magn. Mater. **127**, 273 (1993).

[19] T. Schrefl, R. Fischer, J. Fidler, and H. Kronmüller, J. Appl. Phys. **76**, 7053 (1994).

[20] T. Schrefl, J. Fidler, and H. Kronmüller, CEAM Newsletters **32**, 4 (1994).

[21] R. Fischer, T. Schrefl, H. Kronmüller, and J. Fidler, J. Magn. Magn. Mater. **150**, 329 (1995).

[22] R. Fischer, T. Schrefl, H. Kronmüller, and J. Fidler, J. Magn. Magn. Mater. **153**, 35 (1996).

[23] L. Landau and E. M. Lifshitz, Phys. Z. Sowjetunion **8**, 153 (1935).

[24] W. F. Brown, Jr., Phys. Rev. **58**, 736 (1940).

[25] W. F. Brown, Jr., *Micromagnetics* (Interscience, Wiley, New York, 1963).

[26] N. Kikuchi, *Finite Element Methods in Mechanics* (Cambridge University Press, Cambridge, 1986).

[27] W. Chen, D. R. Fredkin, and T. R. Koehler, IEEE Trans. Magn. **29**, 2124 (1993).

[28] P. E. Gill, W. Murray, and M. H. Wright, *Practical Optimization* (Academic, London, 1981).

[29] W. F. Brown, Jr., J. Phys. Soc. Jpn. **17**, 540 (1962).

[30] W. Döring, in *Handbuch der Physik*, edited by S. Flügge (Springer, Berlin, 1966), Vol. XVII/2.

[31] P. Asselin and A. A. Thiele, IEEE Trans. Magn. **22**, 1876 (1986).

[32] A. Aharoni, IEEE Trans. Magn. **27**, 3539 (1991).

[33] T. Schrefl, J. Fidler, and H. Kronmüller, J. Magn. Magn. Mater. **138**, 15 (1994).

[34] R. Fischer and H. Kronmüller, Phys. Rev. B **54**, 7284 (1996).

[35] A. Arrott and T. Templeton, Physica B **233**, 259 (1997).

[36] P. F. Byrd and M. D. Freedman, *Handbook of Elliptic Integrals for Engineers and Scientists*, 2nd ed. (Springer-Verlag, Berlin, 1971), Vol. 67.

[37] S. Hock, Ph.D. thesis, Universität Stuttgart, Deutschland, 1988.

[38] E. Kneller, *Ferromagnetismus* (Springer, Berlin, 1962).